Heat Transfer Research, 2011, Vol. 42, No. 6

Free Convection in a Vertical Duct: Numerical Study

F. Z. BAKHTI,[1] M. SI AMEUR,[2*] and A. M. CHEHHAT[1]

[1]Department of Mechanics, University of M'sila, Algeria

[2]LESEI Laboratory, Department of Mechanics,
University of Batna (Algeria)

The subject of this paper is a direct numerical study of laminar and laminar-to-turbulent transient natural convection in a vertical duct, with a constant wall temperature, that exceeds the ambient fluid temperature. The governing equations are solved without modeling of the turbulence effect using a finite volume method. We presented the fields of velocity, temperature, and pressure as well as variation of the mean Nusselt number as a function of the Rayleigh number. The numerical simulation has been made for the Rayleigh number in the range from 1 to 10^5 for aspect ratios 3, 5, 8, and 12. The obtained results are compared with those given in the literature and a good agreement has been found.

* * *

Key words: free convection, vertical duct, direct numerical simulation, finite volume method

1. INTRODUCTION

The study of natural heat convection in vertical ducts aroused an interest growing during the last decades. This interest is dictated by the role played by these configurations in many industrial applications in various fields such as cooling of electronic components, air-conditioning, heat exchangers, nuclear thermal power stations, etc.

In the literature, a large number of theoretical and experimental investigations are reported on natural convection in a vertical duct. The seminal work in this field is that of Elenbaas (1942) where an experimental relation between the mean Nusselt number and the channel Rayleigh number was proposed, and this correlation is now often compared with numerical and analytical results in vertical channels. Bodoia and

*Address all correspondence to M. Si Ameur Email: MSIAMEUR@yahoo.fr

ISSN1064-2285

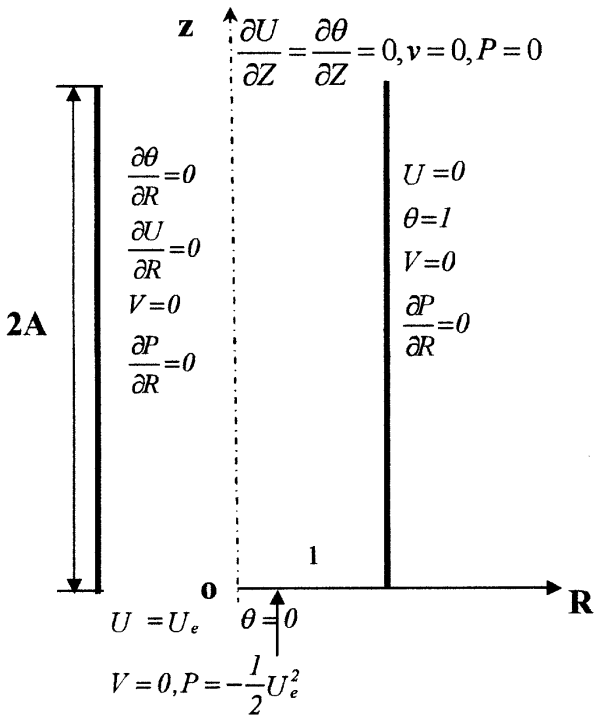

Fig. 1. Studied configuration and boundary conditions.

Osterle (1962) and Aung et al. (1972) have used a numerical method based on finite differences to solve the equations governing laminar natural convection in a parallel-plate vertical flat duct and have compared their results with the values obtained from experimental measurements for the case of constant wall temperature. Marcondes and Maliska (1999) and Desrayaud and Fichera (2002) have used a numerical method based on finite volumes to discretize the elliptic equations governing the natural convection in a vertical duct. Boudebous et al. (2001) have considered the same phenomenon but in a vertical hyperbolic duct with a constant wall temperature, the governing equations are solved by the finite differences method.

Lyons et al. (1991) used the direct numerical simulation (DNS) to solve the equations governing turbulent natural convection with the passive transfer between the walls of the channel. Boudjemadi et al. (1997) and Verstreegh and Nieuwstadt (1998) used the DNS for calculation of turbulent natural convection in a differentially heated vertical duct. Yu et al. (2001) studied the characteristics of an established natural convection turbulent flow in a uniformly heated round tube for a wide range of the Reynolds number and a complete range of the Prandtl number.

In this article, as shown in Fig. 1, we study the laminar and transient turbulent natural convection in a vertical duct of length L, radius R_0, and aspect ratio $A = L/2R_0$, the wall of this duct is maintained at a constant temperature T_p higher than that of the ambient conditions, giving rise to an ascending flow of the air through this duct. In the laminar flow, the numerical simulations were made for the Rayleigh

number between 1 and 10^5 and for various aspect ratios: 3, 5, 8, and 12. For the turbulent flow, we have qualitative results for only one value of the Rayleigh number $\mathrm{Ra} = 10^4$ at $A = 3$. We used the direct numerical simulation (DNS) as a tool of the investigation. The flow is steady in the laminar mode, unsteady in the turbulent mode, two-dimensional and axisymmetric. The fluid is Newtonian, incompressible and obeys the Boussinesq approximation. The thermophysical quantities of the fluid are all assumed to be constant except for the density in the buoyancy force.

2. MATHEMATICAL FORMULATION

With the Boussinesq approximations and assumptions, the dimensionless governing equations can be written as:

the continuity equation

$$\frac{\partial U}{\partial Z} + \frac{\partial V}{\partial R} + \frac{V}{R} = 0 \,, \tag{1}$$

the axial momentum equation

$$\frac{\partial U}{\partial \tau} + U\frac{\partial U}{\partial Z} + V\frac{\partial U}{\partial R}$$

$$= \frac{\partial P}{\partial Z} + \mathrm{Pr}\left[\frac{\partial^2 U}{\partial Z^2} + \frac{1}{R}\frac{\partial U}{\partial R} + \frac{\partial^2 U}{R^2}\right] + \mathrm{Ra}\,\mathrm{Pr}\,\theta \,, \tag{2}$$

the radial momentum equation

$$\frac{\partial V}{\partial \tau} + U\frac{\partial V}{\partial Z} + V\frac{\partial V}{\partial R}$$

$$= \frac{\partial P}{\partial R} + \mathrm{Pr}\left[\frac{\partial^2 V}{\partial Z^2} + \frac{1}{R}\frac{\partial V}{\partial R} + \frac{\partial^2 V}{R^2}\right] - 2\mathrm{Pr}\frac{V}{R^2} \,, \tag{3}$$

the energy equation

$$\frac{\partial \theta}{\partial \tau} + U\frac{\partial \theta}{\partial Z} + V\frac{\partial \theta}{\partial R} = \left[\frac{\partial^2 \theta}{\partial Z^2} + \frac{1}{R}\frac{\partial \theta}{\partial R} + \frac{\partial^2 \theta}{\partial R^2}\right], \tag{4}$$

where Ra and Pr denote, respectively, the Rayleigh number based on R_0 and the Prandtl number. They are defined as:

$$\mathrm{Ra} = \frac{g\beta\Delta T R_0^3}{a\nu} \quad \mathrm{Pr} = \frac{\nu}{a} \,,$$

$$Z = \frac{z}{R_0}, \quad R = \frac{r}{R_0}, \quad U = \frac{uR_0}{a}, \quad V = \frac{vR_0}{a},$$

$$\theta = \frac{T - T_0}{T_p - T_0}, \quad \tau = \frac{ta}{R_0^2}, \quad P = \frac{p^* R_0^2}{\rho_0 a^2}.$$

The other dimensionless variables are defined as follows.

Since the flow is axisymmetric, the following dimensionless boundary conditions for Eqs. (1)–(4) can be adopted:

- laminar flow:

For $Z = 0$ and $0 < R < 1$ (inlet): $U = U_e$, $\theta = 0$, $V = 0$,

$$P = -\frac{1}{2} U_e^2 . \tag{5}$$

For $Z = 2A$ and $0 < R < 1$ (outlet): $V = 0$, $P = 0$,

$$\frac{\partial U}{\partial Z} = \frac{\partial \theta}{\partial Z} = 0 . \tag{6}$$

For $R = 0$ and $0 < Z < 2A$ (symmetry axis): $V = 0$,

$$\frac{\partial U}{\partial R} = \frac{\partial \theta}{\partial R} = \frac{\partial P}{\partial R} = 0 . \tag{7}$$

For $R = 1$ and $0 < Z < 2A$ (wall): $U = 0$, $V = 0$, $\theta = 1$,

$$\frac{\partial P}{\partial R} = 0 . \tag{8}$$

Turbulent flow:

- initial conditions:

$$\tau = 0, \quad U(R, Z, \tau = 0) = U_e, \quad V(R, Z, \tau = 0) = 0,$$

$$T(R, Z, \tau = 0) = \theta_0, \quad P(R, Z, \tau = 0) = 0 , \tag{9}$$

- boundary conditions:

We use the same boundary conditions of the laminar flow; only a white noise is added at the inlet velocity U_e for flow perturbation; then the expression of the inlet velocity becomes:

$$U(R,\ 0,\ \tau) = U_e + 0.1ran\,[(issed) - 0.5]\exp\left[-\frac{R^2}{8}\right]. \tag{10}$$

The inlet velocity U_e constitutes a major problem in the natural convection flows in confined or semi-confined space, we proposed an approximate explicit expression to determine its value based on the equality of the flow rate. This expression is as follows:

$$U_e = 0.5\sqrt{\mathrm{Ra\,Pr}}\ . \tag{11}$$

The mean Nusselt number is given by:

$$\overline{\mathrm{Nu}} = \frac{2R_0}{L}\int_0^1 U\theta R dR\ ,\quad \overline{\mathrm{Nu}} = \frac{1}{A}\int_0^1 U\theta R dR\ . \tag{12}$$

3. RESOLUTION OF THE SYSTEM OF EQUATIONS

The numerical resolution of the equations is based on the finite volume method, the discretization of the equations is completed by using the Power Low Differencing Scheme (PLDS) for the discretization of convection terms and the implicit scheme for the temporal discretization. The algorithm SIMPLE (Semi-Implicit Method for Presses Linked Equation) was adopted to ensure the coupling pressure velocity, and the discretized equations obtained were solved by using the method of sweeping associated with the Thomas algorithm TDMA (Tri-Diagonal Matrix Algorithm).

4. RESULTS AND DISCUSSION

4.1 The Laminar Flow

In the present study, we fixed the ambient temperature at 20°C and that of the wall at 50°C. The conveyed fluid is air. The physical properties of air are chosen by linear interpolation tables at an average temperature equal to 35°C: $\rho = 1.15676$ kg/m^3, $C_p = 1.006228$ J/kg·K, $\nu = 1.65\cdot10^{-5}$ m^2/s, $a = 2.338\cdot10^{-5}$ m^2/s, $\beta = 3.254\cdot10^{-3}$ K^{-1}, $\mathrm{Pr} = 0.71$.

The choice of the grid has a great influence on the precision of the results and the time of computing, in order to optimize these parameters we carried out several simulation tests for various grids: 50 × 50, 100 × 50, 100 × 100, 150 × 50, and 200 × 50.

A grid independence study was performed by examining the impact of the grid size on the mean Nusselt number (the details of the results of the grid independence are given in Table 1).

$$Gap\% = 100\left|\frac{\overline{\mathrm{Nu}}\,(200\times 50) - \overline{\mathrm{Nu}}\,(NI\times NJ)}{\overline{\mathrm{Nu}}\,(NI\times NJ)}\right|\ . \tag{13}$$

Table 1.
Comparison of the mean Nusselt number for various grids at the aspect ratio $A = 3$

Grid $NI \times NJ$	Nu for Ra = 10	Gap %	Nu for Ra = 100	Gap En %	Nu for Ra = 1000	Gap En %
50 × 50	0.4254	2.374	1.4209	2.794	3.1182	3.332
100 × 50	0.4231	1.844	1.4132	2.264	3.1017	2.281
100 × 100	0.4226	1.727	1.4124	2.209	3.0985	2.271
150 × 50	0.4182	0.693	1.3942	0.932	3.0732	1.916
200 × 50	0.4153	–	1.3812	–	3.0143	–

$\overline{\mathrm{Nu}}\,(200 \times 50)$ is taken as a value of reference to calculate the gap expressed as a percentage.

By examining the gap carried out at the Nusselt number values, we selected the grid 150 × 50 which ensures good compromises between the precision of the results and the computing time.

4.1.1 V*elocity and temperature fields*

To visualize the fields of velocity and temperature we represent their profiles at the inlet, center, and outlet from the duct for the aspect ratio A equal to 3, 5, 8, and 12, respectively, and for Ra = 100 and 1000. Figures 2 and 3 represent these profiles (the temperature profiles are on the right and those of velocity are on the left). The velocity profiles presented in Fig. 2 for Ra = 100 are traditional parabolic profiles of the laminar flow in a duct, according to A. We note that neither the geometry dimensions nor the heat transfer within the fluid have an influence on the shape of the velocity profile.

When Ra increases (above 100), as shown in Fig. 3 for Ra = 10^3, the dominant effect of the buoyancy forces along the duct wall induces an acceleration of the fluid near the wall and a deceleration near the axis to satisfy the conservation of mass. We note that for small values of Ra (Ra = 100), the temperature field tends to become homogeneous at the duct exit (Figs. 2c and 4a). This can be explained by the fact that the heat transfer by conduction from the wall prevails over that by convection from the duct entrance.

For high Ra (greater than 100), e.g., Ra = 1000 in Figs. 3c and 4b, the reverse phenomenon is noted. The convective transport of heat dominates the conductive one, which explains the important difference between the temperatures on the axis and on the wall along the duct. We can also note that the effect of the aspect ratio on the profiles of velocity and temperature is significant especially at the inlet from the duct (see Figs. 2a and 3a). This effect disappears with advance along the duct due to the hydrodynamic and thermal effects.

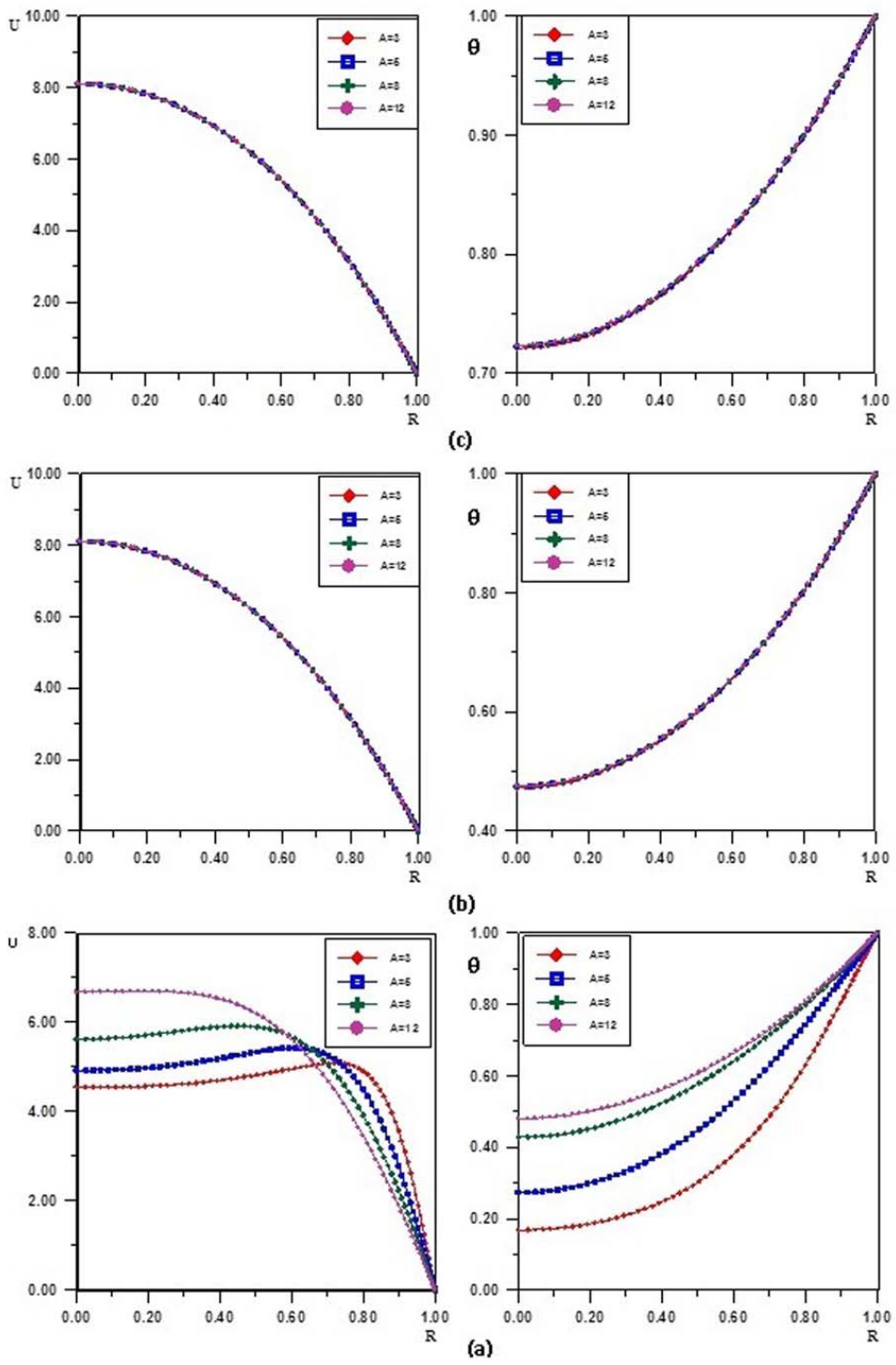

Fig. 2. Velocity and temperature profiles for Ra = 100: a) inlet; b) center; c) outlet.

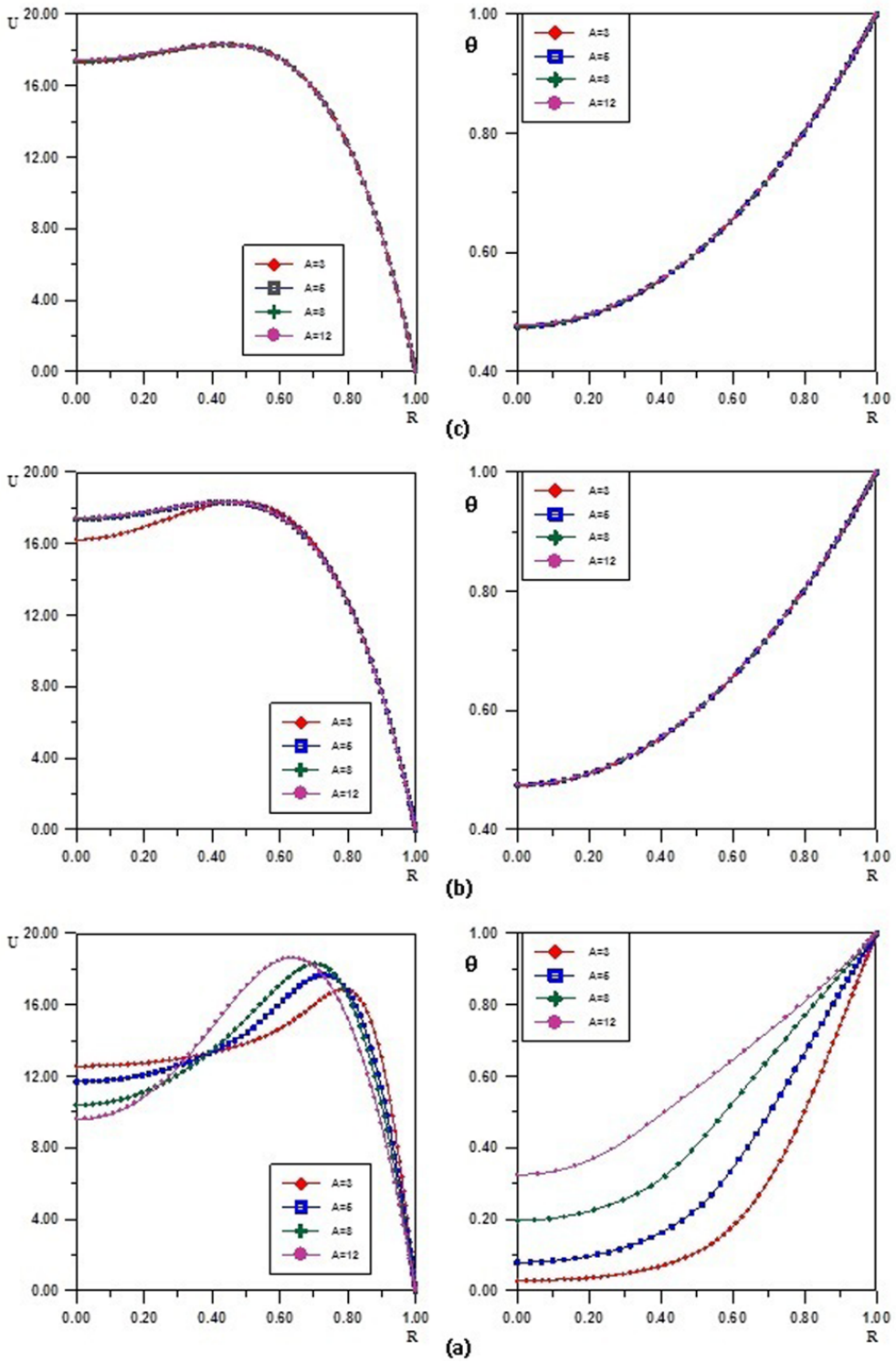

Fig. 3. Velocity and temperature profiles for Ra = 1000: a) inlet; b) center; c) outlet.

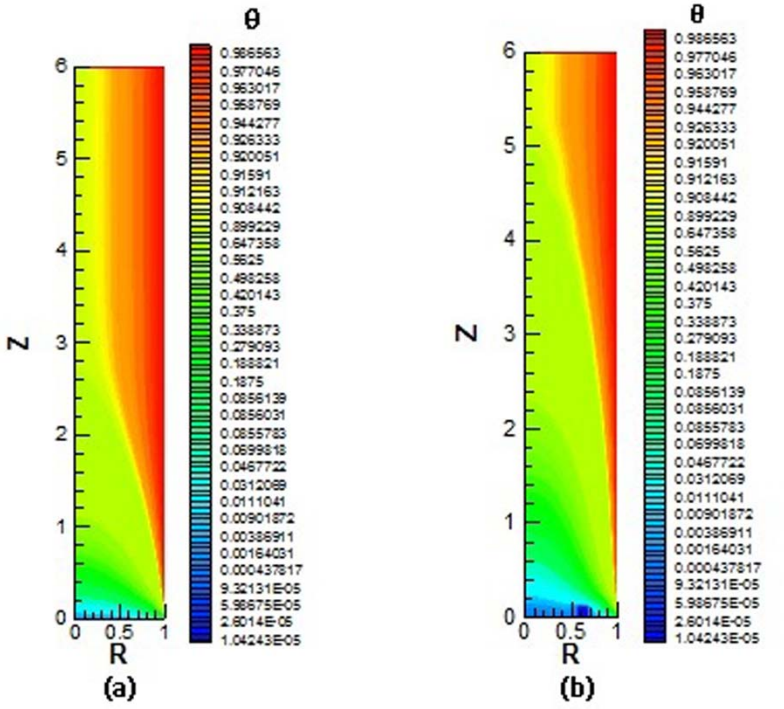

Fig. 4. Temperature field for: a) Ra = 100; b) Ra = 1000.

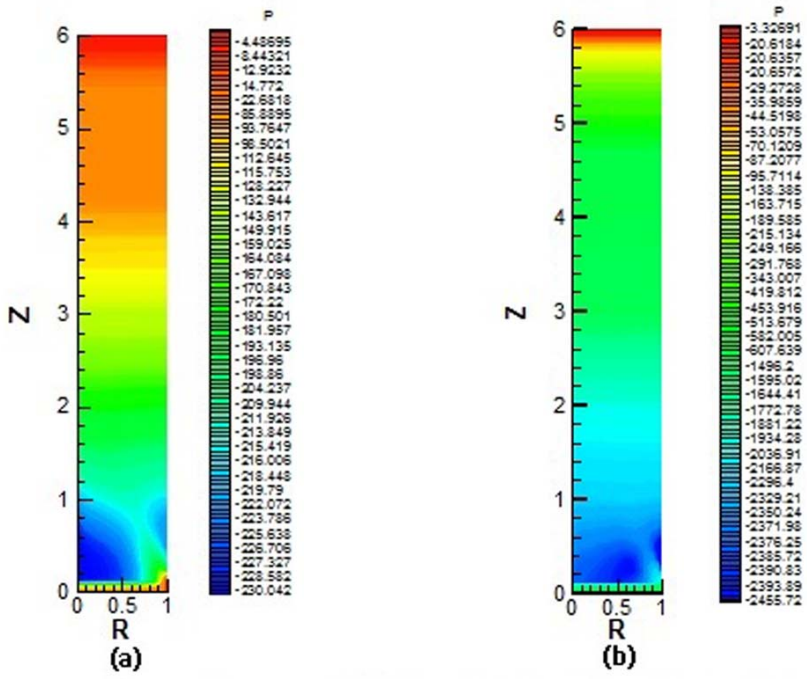

Fig. 5. Pressure filed for: a) Ra = 100; b) Ra = 1000.

4.1.2 *Pressure field*

Figure 6 presents the profiles of pressure along the duct for the Rayleigh number values equal to 100 and 1000 and for A = 3, 5, 8, and 12. In Figures 5 and 6, we note that neither the Rayleigh number nor the aspect ratio A influence the shape of the pressure profile. The pressure increases at the inlet to the duct, passes the maximum, and then decreases gradually to satisfy the condition at the outlet (P = 0). The value of this maximum increases as Ra and A increase.

4.1.3 *Validation*

Figure 7 shows the mean Nu number as a function of the Rayleigh number Ra. Our results for A = 3 are compared with the literature results. The models of Elenbaas (1942), Churchill (1977), and Raithby and Hollands (1985) are compared with the experimental results of Elenbaas (1942) and those of the numerical simulations by Bodoia and Osterle (1962) and Miyataka and Fujii (1973). We can note that all these layouts are limited by the model of Churchill (1977) which presents the lower limit and by the experimental values of Elenbaas (1942) for low values of the Rayleigh number, and the Raithby and Hollands (1985) model for high Ra values.

Figure 7 shows clearly a good agreement between all these results, with a maximum change of 16% between the lower and higher limits. Our numerical results are very close to the results of Churchill (1977), which proves the reliability of the computer code. This program has been also successfully applied in the previous study of mixed convection in an inclined thick duct (Bakhti and Si Ameur, 2011).

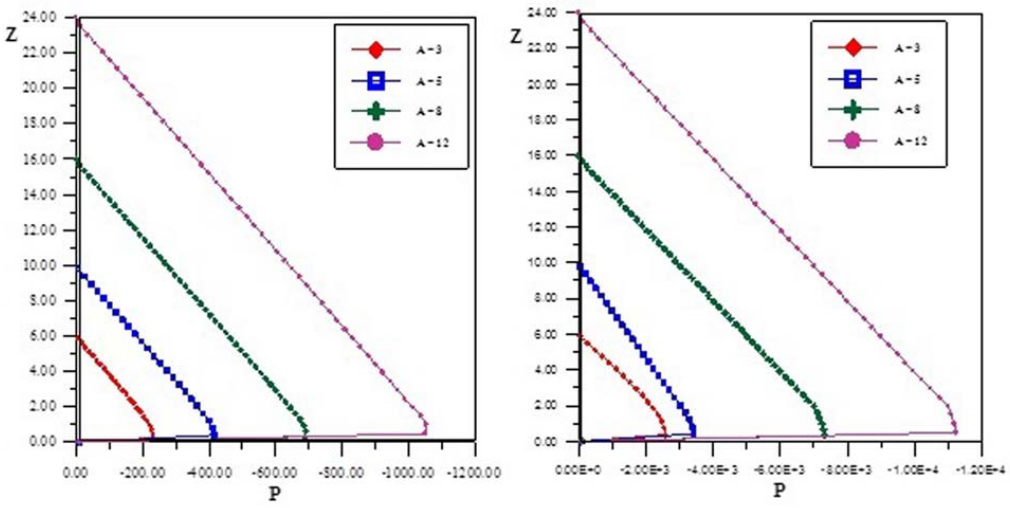

Fig. 6. Pressure evolution along the duct for: a) Ra = 100; b) Ra = 1000.

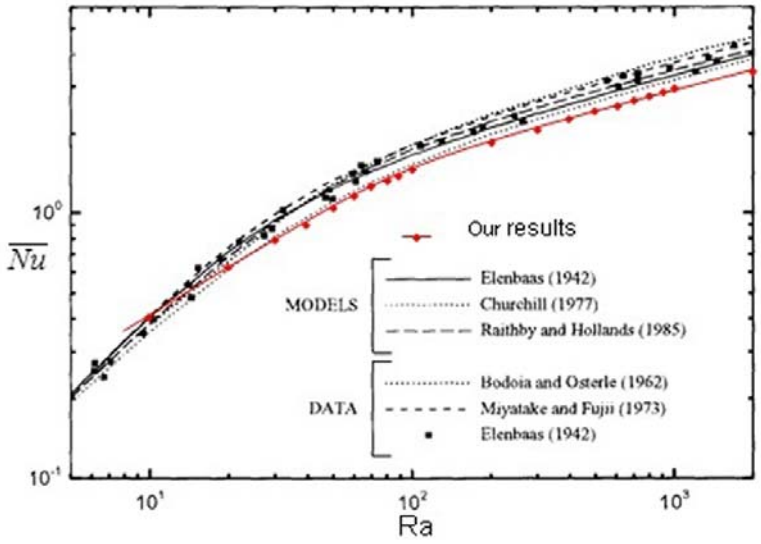

Fig. 7. Variation of the mean Nusselt number as a function of the Rayleigh number.

4.2 Turbulent Flow

We fixed the ambient temperature at 20°C and that of the wall at 56°C; the characteristics of the air are estimated at an average temperature equal to 38°C: ρ = 1.136 kg/m^3, C_p = 1.006228 J/kg·K, $\nu = 1.68 \times 10^{-5}$ m^2/s, a = 2.366×10^{-5} m^2/s, $\beta = 3.22 \times 10^{-3}$ K^{-1}, Pr = 0.71.

After several numerical tests, we fixed for our numerical simulations the aspect ratio A = 3, the Rayleigh number Ra = 10^4, and a space resolution of 1000 × 200 points of the grid and an increment of time:

$$\Delta\tau = \Delta Z / U_e .$$

4.2.1 *Velocity and temperature fields*

Figure 8 presents the velocity and temperature profiles at the inlet, center, and outlet from the duct. The velocity decreases less quickly when we deviate from the axis, it remains rather close to its maximum value on a significant part of the section, after which it falls very quickly when we approache the wall. We see that the turbulent flow is characterized by an almost uniform velocity along the duct because the intense exchange of fluid momentum between particles is due to turbulence.

We note a definitely stronger temperature variation as compared to the laminar flow. The development of a vortex in a turbulent flow facilitates the setting of different temperatures on contact with the fluid and gives place to significant gradients.

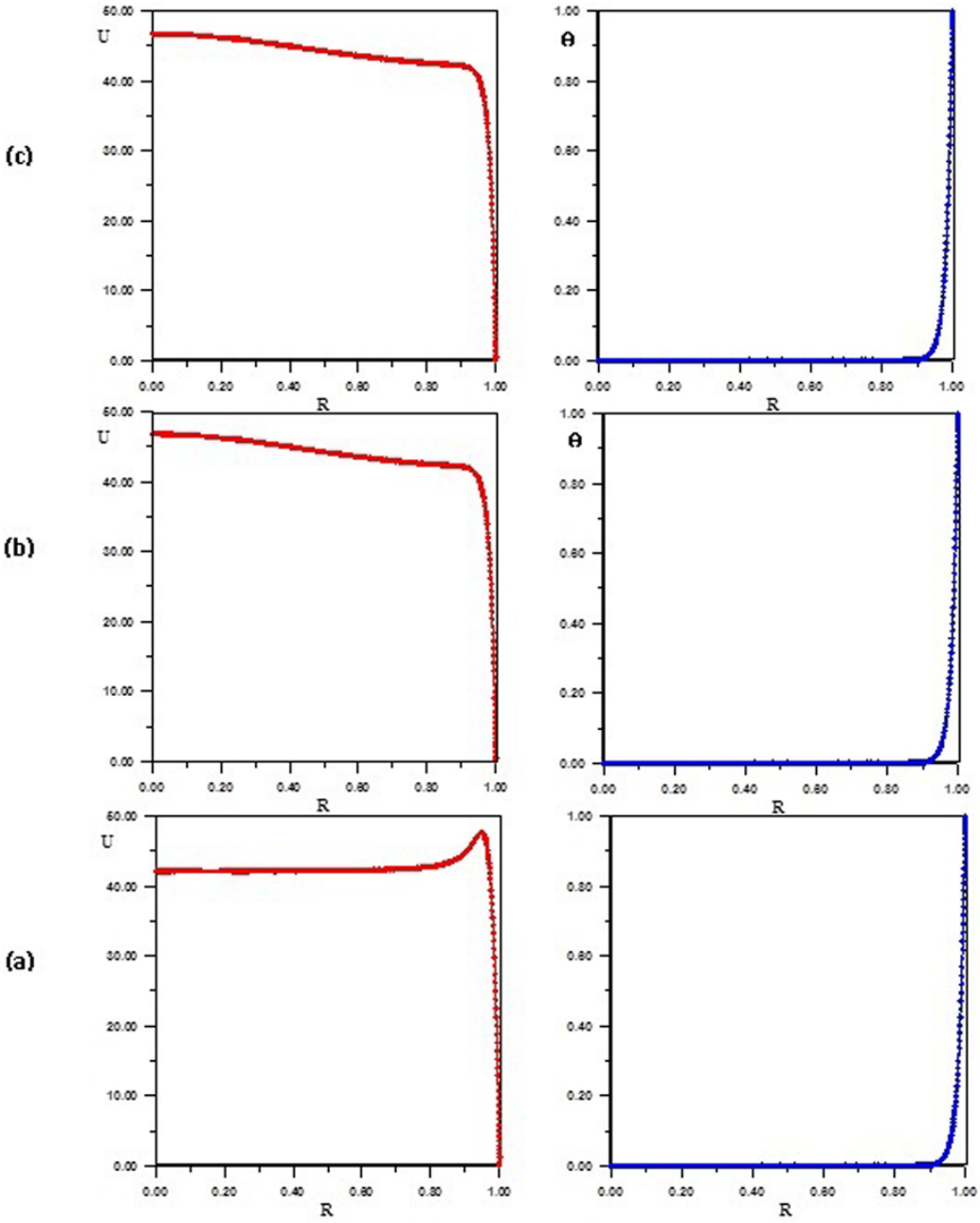

Fig. 8. Average velocity and temperature for Ra = 10^4: a) inlet; b) center; c) outlet.

Despite the presence of vortex instabilities that can be observed in Fig. 10, we note that the field of temperature is only transported and diffused by the flow, which implies that the field of temperature is a passive scalar.

4.2.2 *Pressure field*

Figure 9 illustrates the evolution of the pressure along the duct for Ra = 10^4 and A = 3. It is interesting to note that the pressure profile presents the same tendency of evolution of the laminar flow. The pressure increases at the inlet to the duct, passes the maximum, and then decreases gradually to satisfy the condition at the outlet ($P = 0$). We can conclude that the mode of flow does not have a great influence on the pressure profile.

4.2.3 *Vorticity field*

Figure 10 presents temporal sequences of the vorticity contours; we note that initially the flow field is irrotational, but after a certain period of time vortices of various size develope along the duct, come from flow instabilities particularly at the points of inflection at the level of the velocity profile. While the flow develops, the vorticity concentrates in the region near the axis of symmetry of the duct. That is due to the fact that a part of the produced turbulent kinetic energy near the wall is very quickly destroyed locally, the other part is transported towards the downstream and diffused at the same time at the center of the tube.

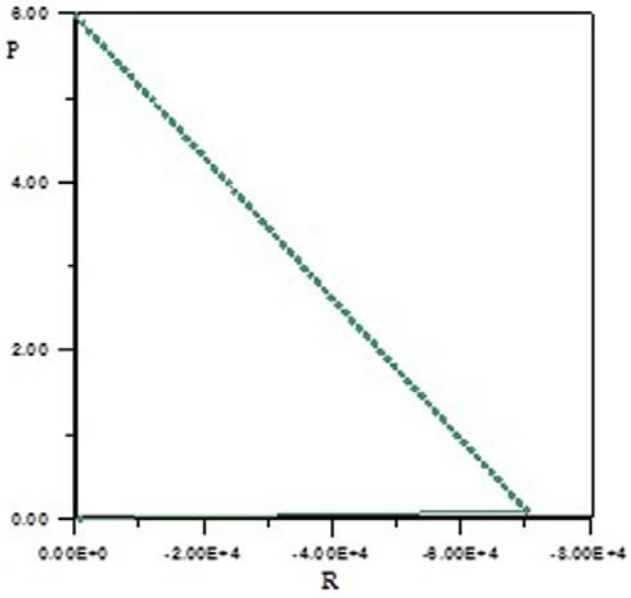

Fig. 9. Average pressure evolution along the duct for Ra = 10^4.

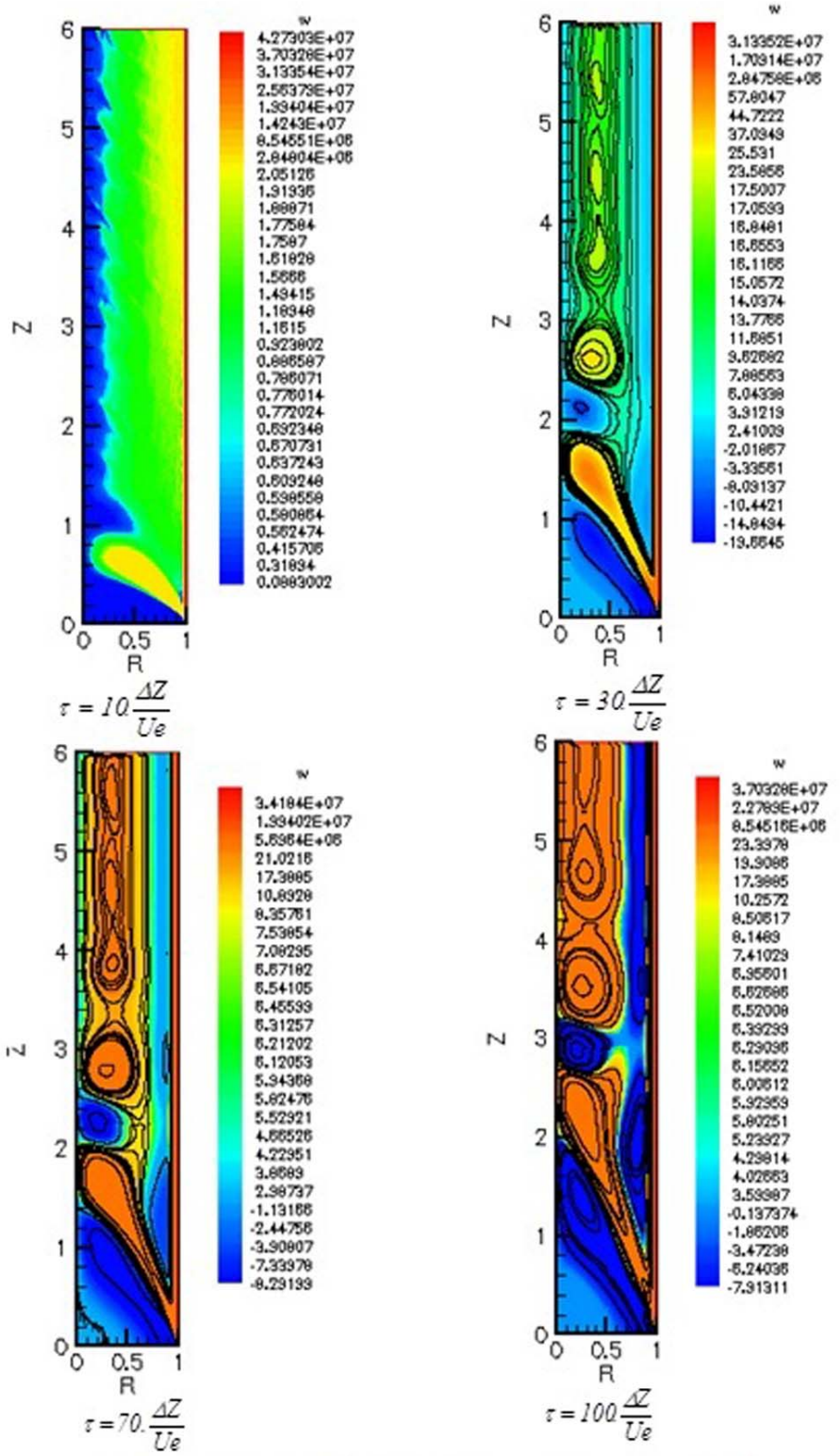

Fig. 10. Velocity field at A = 3 and Ra = 10^4.

5. CONCLUSIONS

The study presented in this article is aimed at better including/understanding the process of the natural, laminar, and turbulent convection in a vertical duct, whose wall is maintained at a constant temperature higher than that of the ambient conditions giving rise to an ascending convective flow of air through this duct. We presented the hydrodynamic and thermal fields including the variation of the mean Nusselt number as a function of the Rayleigh number for various aspect ratios A. The numerical simulations were made for the Ra number between 1 and 10^5, A = 3, 5, 8, and 12. The effect of the aspect ratio A is observed at the inlet to the duct, it decreases while advancing along duct because of the hydrodynamic and thermal establishment of this flow.

In the second part of this work, we examined the turbulent natural convection by using the direct numerical simulation (DNS), we also presented the hydrodynamic and thermal fields for only one value of the Rayleigh number Ra = 10^4 and that for A = 3. Instabilities of the turbulent flow develop with time and give rise to vortices. We studied the dynamics of this formation using vorticity visualization. It is difficult to simulate turbulent heat convection even with the use of a personal computer for DNS. The obtained results encourage us to improve the computer program for treating turbulent thermal and dynamic fields in others similar configurations.

NOMENCLATURE

A	aspect ratio of the duct
a	thermal diffusivity, = $k / \rho C_p$, $m \cdot s^{-2}$
C_p	specific heat at constant pressure, $J \cdot kg^{-1} \cdot K^{-1}$
g	acceleration of gravity, $m \cdot s^{-2}$
L	duct length, m
Nu	Nusselt number, = d / λ
p	pressure, Pa
P	dimensionless pressure
p^*	driving pressure, Pa
Pr	Prandtl number, = ν / a
r	radial coordinate, m
R	dimensionless radial coordinate
R_0	radius of the duct, m
Ra	Rayleigh number, = Gr Pr
t	time, s
T	temperature, K
T_0	ambient temperature, K
T_p	wall temperature, K
u	axial velocity, $m \cdot s^{-1}$
U	dimensionless axial velocity

U_e	dimensionless inlet velocity
v	radial velocity, m·s^{-1}
V	dimensionless radial velocity
z	axial coordinate, m
Z	dimensionless axial coordinate

Greek symbols

β	isobaric coefficient of fluid thermal expansion
ΔT	temperature variation, K
θ	dimensionless temperature
ν	kinematic viscosity, m2·s^{-1}
ρ	density, kg·m^{-3}
ρ_0	density at T_0, kg·m^{-3}
τ	dimensionless time.

REFERENCES

Aung, W., Fletcher, L. S., and Sernas, V., Developing laminar free convection between vertical flat plates with asymmetric heating, *Int. J. Heat Mass Transfer*, vol. 15, pp. 2293–2308, 1972.

Bakhti, F. Z. and Si Ameur, M., Numerical simulation of mixed convection in an inclined thick duct, *J. Eng. Sci. Technol. Rev.*, vol. 4, no. 2, pp. 152–159, 2011.

Bodoia, J. R. and Osterle, J. F., The development of free convection between heated vertical plates, *Trans. ASME, J. Heat Transfer*, vol. 84, no. 1, pp. 40–44, 1962.

Boudebous, S., Meniai, A. H., and Nemouchi, Z., Numerical study of developing natural laminar convection in a vertical hyperbolic duct of a fixed length and with a constant wall temperature, *Numer. Heat Transfer*, vol. 40, pp. 783–800, 2001.

Boudjemadi, R., Maupu, V., Laurence, D., and Quere, P. L., Budgets of turbulent of stresses and fluxes in vertical slot natural convection flow at Rayleigh Ra = 10^5 and $5.4{\cdot}10^5$, *Int. J. Heat Fluid Flow*, vol. 18, pp. 70–79, 1997.

Churchill, S. W., A comprehensive correlating equation for buoyancy-induced flow in channels, *Lett. Heat Mass Transfer*, vol. 4, pp. 193–199, 1977.

Desrayaud, G. and Fichera, A., Laminar natural convection in a vertical isothermal channel with symmetric surface-mounted rectangular rib, *Int. J. Heat Fluid Flow*, vol. 23, pp. 519–529, 2002.

Elenbaas, W., Heat dissipation of parallel plates by free convection, *Physica*, vol. 9, no. 1, pp. 1–28, 1942.

Lyons, S. L., Hanratty, T. J., and McLaughlin, J. B., Direct numerical simulation of passive heat transfer in a turbulent channel flow, *Int. J. Heat Mass Transfer*, vol. 34, pp. 1149–1161, 1991.

Marcondes, F. and Maliska, C. R., Treatment of the inlet boundary conditions in natural convection flows on open ended channels, *Numer. Heat Transfer*, vol. 35, pp. 317-345, 1999.

Miyataka, O. and Fujii, T., Free convective heat transfer between vertical parallel plates, *Kagaku*, vol. 36, pp. 405–412, 1972.

Raithby, G. D. and Hallands, K. G. T., Natural convection, in: W. M. Rohsenow, J. P. Hartnett, and E. M. Granic (Eds.), *Handbook of Heat Transfer Fundamentals*, Ch. 6, pp. 34–36, New York, McGraw-Hill: McGraw, 1985.

Verteegh, T. A. M. and Nieuwstadt, F. T. M., Turbulent budgets of natural convection in infinite, differentially heated, vertical channel, *Int. J. Heat Fluid Flow*, vol. 19, pp. 135–149, 1998.

Yu, B., Ozoe, H., and Churchill, S. W., The characteristics of fully developed turbulent convection in a round tube, *Chem. Eng. Sci.*, vol. 56, pp. 1781–1800, 2001.

□◆◆◆□